

Tuning the selectivities of Mg-Al mixed oxides for ethanol upgrading reactions through the presence of transition metals

Jorge Quesada, Laura Faba, Eva Díaz, Salvador Ordóñez*

Department of Chemical and Environmental Engineering, University of Oviedo, c/ Julián Clavería, s/n, 33006, Oviedo, Spain

ARTICLE INFO

Keywords:

Butanol
Cobalt
Nickel
Dehydrogenation
Hydrogenation
Aldol condensation

ABSTRACT

The effect of the presence of reduced Co and Ni (chosen as representative metals because of their good activity for dehydrogenation reactions) on the catalytic performance of basic mixed oxide (Mg-Al) for ethanol condensation is studied in this work. This effect has been studied both in absence and in presence of hydrogen, and considering the different steps of this complex reaction. Globally, best results were obtained with Co/MgAl, under reducing atmosphere, at mild temperature (below 600 K). At these conditions, 1-butanol production rates are up to eight times higher than the obtained with Mg-Al under inert atmosphere. Co has a marked activity in the dehydrogenation step, that prevails over its less relevant activity in aldolization and hydrogenation reactions. This result indicates the relevant role of this first reaction step. DRIFT spectroscopy analyses were carried out to support the experimental results and to identify the role of hydrogen and metals on the oligomerization and permanent adsorption processes, which can produce the deactivation of the catalyst.

1. Introduction

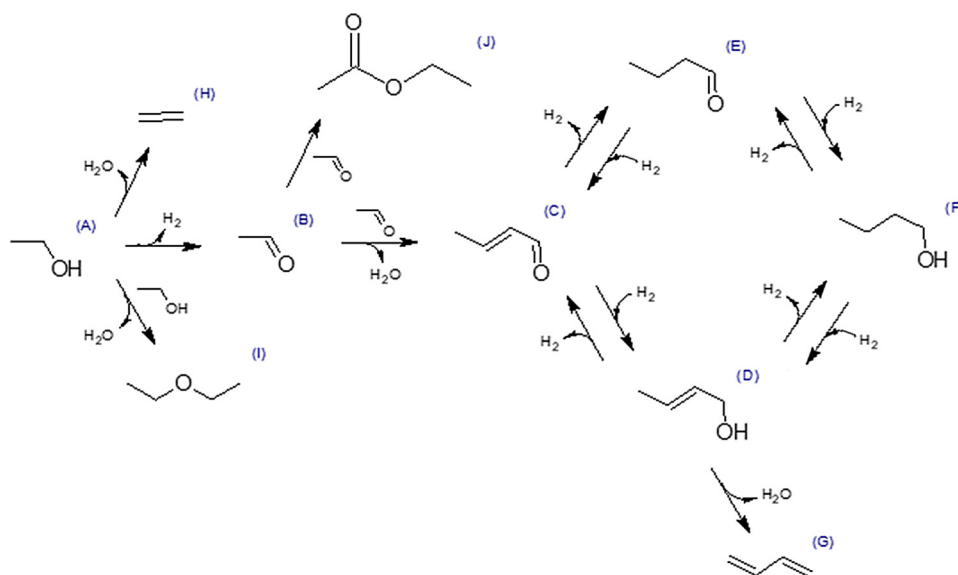
Gas-phase ethanol condensation has been intensively investigated in the last few years, because of the high potential of ethanol as bioplat-form molecule [1–4]. Among the different chemicals obtained from ethanol [5–8], 1-butanol is the most valuable one, with better fuel properties than ethanol, and many uses as solvent and platform molecule. There is not agreement about the actual mechanism for 1-butanol formation. The so-called four-step mechanism (Scheme 1) is the most accepted one, although several authors also suggest the direct ethanol condensation or the acetaldehydeethanol reaction [4,9–11]. According to the four-step mechanism, acetaldehyde aldolization is usually considered as the rate-determining step since it involves two molecules, and different active sites, requiring an appropriate balance between acid and medium-strength basic sites. Different materials, mainly mixed oxides and hydroxyapatites (HPA) have been proposed as promising catalysts [4,11,12]. Despite their good activity for aldolization, experimental results indicate that the difficulty in activating the α -hydrogen of the ethoxides (previous ethanol dehydrogenation) strongly limits the final yields [13–15]. This effect was previously observed for the dehydrogenation of different alcohols, the use of transition metals in the reduced form (Co, Ni, Cu, Fe, Ir, etc.) being proposed for reducing the activation energy of the α CH bond scission [16,17]. In addition, reduced metals are supposed to alter the acid/base sites distribution in a lower extent than the metal oxides.

Under inert conditions, or in absence of any active metal for the molecular hydrogen activation, once the acetaldehyde reacts producing crotonaldehyde, the 1butanol is obtained upon two subsequent hydrogenations: terminal C=O bonds hydrogenation through the Meerwein-Ponndorf-Verley (MPV) reduction (crotonaldehyde and butanal), and hydrogenation of the unsaturated intermediates (crotonaldehyde and crotyl alcohol) by surface-mediated hydrogen transfer reaction [6,9]. Under these conditions, ethanol molecules are the hydrogen source for the former hydrogenation [18], being the hydrogen released in the dehydrogenation step [15,18,19]. HPA and mixed oxides are not very active for these reactions, so the global process is still far to be optimized.

This work is focused on the study of the effect of supporting transition metals and including hydrogen in the feed on the performance of Mg-Al mixed oxides for ethanol gas-phase condensation. It was previously suggested that the use of reducing conditions, in addition to the expected improvement in hydrogenation steps, has a positive effect on the catalyst stability, preventing the permanent deposition of unsaturated molecules [20]. Mg-Al mixed oxide was chosen as bulk material, considering the well-known behaviour of this material for this reaction [6]. The idea of using metal-modified oxides has been previously proposed by some authors, studying the effect on the upgrading of different alcohols, such as methanol or ethanol [21–23]. In this context, Co and Ni are good candidates because of their high activity for alcohol dehydrogenations [23,24]. However, most of the reported

* Corresponding author.

E-mail address: sordonez@uniovi.es (S. Ordóñez).



Scheme 1. Reaction mechanism for the gas phase ethanol upgrading [5–8]. Symbols: (A) ethanol; (B) acetaldehyde; (C) crotonaldehyde; (D) crotyl alcohol; (E) butanal; (F) 1-butanol; (G) 1,3-butadiene; (H) ethylene; (I) diethyl ether; (J) ethyl acetate.

studies are performed with very high metal loadings (15–20 %), masking the original acid-basic properties of the bulk material.

Thus, the aim of this work is to study the role of Co and Ni as reduced nanoparticles in the promotion of the steps catalyzed by these metals, but affecting, as little as possible, the acid-basic properties of the original bulk material (Mg-Al). We propose catalysts with only 1 wt. % of metal, prepared by surface deposition. This procedure is typically used with noble metals, but not so often for transition ones. In fact, in most of the works reported, the metal is introduced into the bulk structure, modifying the original coordination lattice by substituting the original cations [25,26]. The second modification proposed in this work is to feed controlled amounts of hydrogen, in order to both, keep reduced these nanoparticles, and to improve their performance in hydrogenation steps. This idea is supported by our previous studies with Au/TiO₂ for this reaction, obtaining an improvement of 74% in the conversion and almost 10% in the 1-butanol selectivity when working in presence of H₂ [27].

2. Experimental methods

2.1. Catalysts preparation

Mg-Al mixed oxide (Mg/Al = 3) was obtained by the calcination of the corresponding hydrotalcite, prepared by coprecipitation of the Mg and Al nitrates (Aldrich magnesium nitrate hexahydrate, and Aldrich aluminium nitrate nonahydrate) at low super-saturation and under sonication. The detailed procedure is reported in the literature [6]. The gel was precipitated by increasing the pH to 10 with a NaOH solution (10 wt.%) and it was aged at 353 K for 24 h. The solid phase was centrifuged, washed with deionized water to pH 7 and dried at 383 K for 24 h, yielding the hydrotalcite (HT). Finally, the mixed oxide was obtained by calcining the HT in flowing air, from 293 to 973 K with a temperature rate of 5 K min⁻¹, holding this setpoint for 5 h.

The Ni/Mg-Al and Co/Mg-Al materials (1 wt.% of metal) were synthesized by incipient wetness impregnation, using nickel (II) nitrate 6-hydrate (Panreac), and cobalt (II) nitrate 6-hydrate (Panreac). After the impregnation, the catalysts were treated under airflow from 293 to 973 K with a temperature ramp of 5 K min⁻¹, holding this temperature for 5 h, in order to remove the precursor salts. The reduced metals were obtained by treating the materials in flowing H₂/Ar mixture (10 vol. % of H₂; 20 mL min⁻¹) at 823 K for 6 h, according to the results observed during the characterization of the calcined precursors. In order to avoid

further metal re-oxidation, the reduction was performed in-situ before each experiment.

2.2. Catalysts characterization

Temperature-programmed reduction analyses (TPR) were carried out in a Micromeritics 2900 TPD/TPR instrument, in order to define the reduction temperature of the catalysts precursors. In good agreement with the typical procedure, 10 mg of calcined catalytic precursors were treated under H₂ flow (10 vol.% H₂/Ar) from 298 to 973 K, with a temperature rate of 2.5 K min⁻¹. Once the final catalysts were obtained, morphologic properties were determined by N₂ physisorption at 77 K in a Micromeritics ASAP 2020 using the Brunauer-Emmett-Teller (BET) method to analyse the surface area, and the Barret-Joyner-Halenda (BJH) method to calculate the pore volume and diameter. Surface basicity and acidity were analysed by temperature programmed desorption (TPD) using a Micromeritics 2900 TPD/TPR. 10 mg were pre-treated in He flow and saturated with CO₂ or NH₃ to determine the basicity or acidity, respectively. The evolution of CO₂ and NH₃ signals were followed in a Pfeiffer Vacuum Omnistar Prisma mass spectrometer, as well as the temperature was increased at 2.5 K min⁻¹ between 298 and 973 K.

The crystallographic structure of the catalysts was determined by X-ray diffraction (XRD) using a Philips PW 1710 diffractometer with a CuKα line (1.54 Å) in the 2θ range within 5 and 80° at 2° min⁻¹ of scanning rate. High-resolution transmission electron microscopy (HRTEM) analyses of the fresh materials were carried out to determine the nanoparticle size and distribution, as well as the metal dispersion, in a JEOL JEM2100 instrument. H₂ chemisorption was also performed in order to determine the metal dispersion and the crystallite size of the fresh and used catalysts, using the same instrument as for the morphological study (Micromeritics ASAP 2020).

2.3. Catalytic studies

Activity experiments were carried out from 523 to 723 K (with steps of 50 K) in a 0.4 cm i.d. U-shaped fixed bed quartz reactor located inside a controlled electric furnace. The catalyst (150 mg; 250–355 μm) was placed above a quartz wool plug. The sample was pre-treated at 473 K for 1 h in flowing He before each experiment. Absolute ethanol was supplied with a syringe pump in the He or H₂-He (10 vol.% of H₂) flow, causing the in situ vaporization, obtaining a 32 vol.% of ethanol, fed to

the reactor at 20 mL min⁻¹ (STP). These conditions were chosen according to the optimization reported in our previous work and they correspond to a weight hourly space velocity (WHSV) of 7.9 h⁻¹ [20]. The outlet gases were on-line analysed with a HP6890 Plus gas chromatograph with a flame ionization detector (GC-FID), using a TRB-5MS capillary column. Additional GC-FID analyses were off-line performed combining two columns (HP-Plot Q and HPPlot MoleSieve 5 A) in order to distinguish and quantify ethylene and methane. Products identification was performed using commercial standards and supported by GC-MS (Shimadzu QP-2010) by the same methodology in the GC-FID. Operation conditions were selected in order to ensure that the reported experiments are performed under kinetic regime, being mass transfer effect negligible.

Conversions (x) were calculated from the ethanol concentrations at the reactor inlet and outlet. Carbon balances were calculated by contrasting the total quantity of carbon atoms at the reactor inlet and outlet, taking into account only the identified products (compounds in Scheme 1). Yield was calculated by the following equation:

$$\eta_i(\%) = \left(\frac{\text{moles of ethanol fed converted to the product } i}{\text{moles of ethanol fed}} \right) \cdot 100 \quad (1)$$

The productivity of the different compounds (P_i) during the reaction (average formation rate) were determined as follows:

$$P_i (\text{mmol} \cdot \text{s}^{-1} \cdot \text{g}_{\text{cat}}^{-1}) = \frac{F \cdot x \cdot \phi_i}{W} \quad (2)$$

F = ethanol molar flow fed to the reactor (mmol s⁻¹)

W = catalyst mass (g)

φ_i = Selectivity for product i (moles of ethanol fed converted to a product i/ moles of converted ethanol).

Diffuse reflectance infrared Fourier transform (DRIFT) spectroscopy experiments were performed using a Thermo Nicolet Nexus FTIR equipped with a Smart Collector Accessory and a MCT/A detector. The material (20 mg) was placed inside the catalytic chamber where the temperature was controlled. The sample was pre-treated at 473 K for 1 h in He flow. Spectra were acquired in the 4000-650 cm⁻¹ wavenumber range, after subtraction of the KBr standard background. Spectra were recorded at same temperatures as in the reactor allowing the comparison between both results, and working under inert (He) or reducing conditions (10 vol.% H₂/He), as needed. Signals were transformed to Kubelka-Munk units to obtain semiquantitative results. This method allows quantitatively analyze the amount of adsorbed species on the surface, being the signal (for a same support and comparing analogous conditions) proportional to the concentration of adsorbed species [28].

3. Results and discussion

3.1. Characterization of fresh catalysts

The morphological properties and surface chemistry of parent and metal-modified materials have been analyzed by N₂ physisorption, CO₂-

TPD and NH₃-TPD, being the main results summarized in Table 1. No significant changes in surface area were observed, with only the expected slight decrease after the metal deposition on the parent mixed oxide. In good agreement, pore volume and diameter also slightly decrease. Metals mainly are deposited on acid sites [29,30], being the strongest ones the most affected by the metal deposition. A very similar behavior, disappearing more than 85% of the initially present was observed in both cases. As to the basicity, the decrease respect to the Mg-Al is less marked, being only relevant in the case of the strongest sites. This phenomenon is more evident in the case of Ni material, catalyst that only keeps the weak basic sites.

XRD analyses (Fig. S1) corroborate that there are not significant changes in the general structure of the bulk Mg-Al oxides, the same peaks for all the metal-modified catalysts being observed. Periclase is the main phase in all the cases, with similar diffraction patterns for all the catalysts. No signals related to the added metal species were detected, as expected considering the low metal content. HRTEM analyses were carried out in order to determine the metal particle size and dispersion. Representative histograms of crystallite sizes distributions are depicted in Fig. 1 (corresponding micrographs are included in the Supplementary information, Fig. S2); whereas crystallite sizes and metal dispersion data are summarized in Table 1. A very high dispersion is observed (> 75% in both the cases), with nanoparticles around 1.3 nm large. These values are in good agreement with those reported in the literature for similar catalysts prepared by this procedure [31].

The low crystallite sizes observed by HRTEM suggest a strong interaction between metal and support. This hypothesis is congruent with the high reduction temperatures observed in the TPR results (Fig. 1c). According to the literature, the reduction of Ni nanoparticles takes place at 640 K [32], whereas in our sample metal is mainly reduced at 698 K, with only a minor shoulder at 640 K. The reaction from Co₃O₄ to Co is reported at T ≤ 623 K when is supported over alumina, and peaks around 773 K or above are associated with the reduction of CoAl mixed oxides [33]. Observing the TPR results obtained with the Co/MgAl material, two peaks are highlighted at 565 and 750 K, which are related to the former and the latter reductions, respectively.

3.2. Reaction results under reducing atmosphere

The role of Co and Ni was studied by introducing hydrogen in the helium stream (10 vol.% of H₂). In a previous blank experiment (without catalyst), ethanol conversions were negligible at the temperature range considered in this article, so reported data are directly related to the catalytic activity. The reducing conditions are expected to promote the hydrogenation steps of the reaction mechanism, enhancing the 1-butanol yield, and to hinder oligomerization that could strongly affect to the catalytic stability.

The evolution of the conversion, carbon mass balance and selectivity to the main compounds with the reaction temperature is showed in Fig. 2 for the different tested materials (Mg-Al, Co/Mg-Al and Ni/Mg-Al). Reactions with Mg-Al are also considered in order to analyze any change in the basis mechanism because of the presence of

Table 1

Main results of the fresh catalysts characterization: morphological properties, density and distribution of the acid and basic sites, and HRTEM results. *Results taken from a previous work [20].

Catalyst	Morphological properties			Acid sites (μmol g ⁻¹), [T (K)]			Basic sites (μmol g ⁻¹), [T (K)]			HRTEM	
	S (m ² g ⁻¹)	D _p (Å)	V _p (cm ³ g ⁻¹)	weak	medium	strong	weak	medium	strong	Metal dispersion (%)	Crystallite diameter (nm)
Mg-Al*	226	135	0.7	11.3	12.5	41.8	49.7	71.7	238.6	-	-
				[345, 370]	[450]	[630, 800]	[340]	[400]	[630, 670, 800]		
Ni	182	59	0.4	3.9	3.3	4.0	55.8	10.6	-	78.6	1.3
				[329, 365]	[419]	[517]	[328, 377]	[430]			
Co	207	60	0.4	2.9	3.1	5.4	51.0	70.2	53.8	78.7	1.3
				[325, 358]	[408]	[508]	[355]	[415, 491]	[607, 738]		

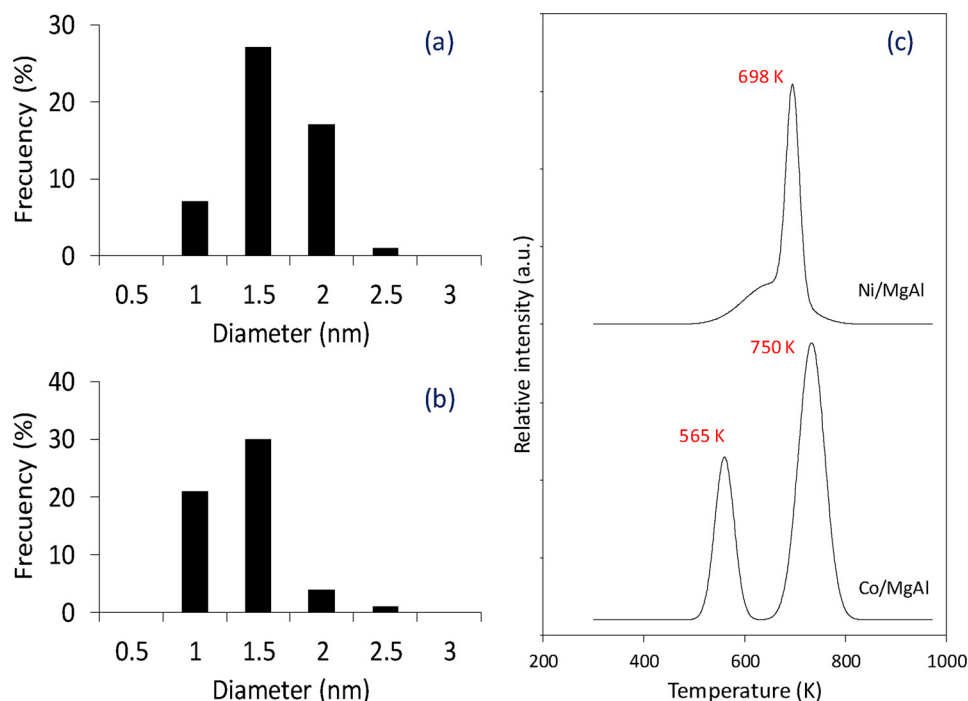


Fig. 1. (a) HRTEM histograms of crystallite diameter of Ni/MgAl (100 particles); (b) HRTEM histograms of Co/MgAl (100 particles); (c) TPR results obtained for Ni/Mg-Al and Co/Mg-Al materials.

H₂ in absence of any metal. The evolution of other intermediates, obtained at lower but measurable concentrations, is included in the Supplementary Data (Table S1). In all the cases, data reported is the average results after three experiments, observing good reproducibility. The decarbonylation of acetaldehyde, reaction catalyzed by several metals [34], is discarded in these cases, since the highest yield to methane obtained was always lower than 0.2% (value observed with Co/MgAl at 723 K).

At the lowest temperatures, conversions obtained with and without metal are very similar, these differences increasing as temperature increases. Thus, conversions of 54.6 (Ni) and 56.3% (Co) are obtained at 723 K, corresponding to relative increments higher than 25% in comparison to those obtained with the MgAl (43.1% at 723 K). These results indicate that metal nanoparticles play a relevant role at reducing conditions. Concerning to the carbon balance, values higher than 80% were obtained for Ni and Co materials at temperatures lower than 700 K, whereas at 723 K they decrease to close to 70%. At same conditions, the value reached with MgAl was 76.2%. These slight differences are related to the lower activity observed with the bulk material, being the production of higher alcohols (> C₄) at highest temperatures the main reason of the decrease with the metal modified ones. These compounds were detected by the GC, but their low individual amount prevents its exact quantification. However, the better carbon balance closures obtained with the metal modified materials at temperatures lower than 700 K suggest a higher global selectivity to the main reaction pathway.

Regarding the selectivity to different reaction products, a positive effect of reducing conditions is clearly observed by comparing the lower selectivity to acetaldehyde obtained with both, Ni and Co materials (in contrast to the parent mixed oxide, at all the temperatures tested); and the higher selectivities obtained for 1-butanol (Fig. 2b). In fact, 1-butanol selectivity reaches maximum values close to 33% with Co and Ni, whereas the maximum selectivity obtained for the bulk material is lower than 23% (results at 623 K for all the materials). These results are considerably higher than other previously published working with Co in larger amounts (higher than 10%) and higher pressures (8% butanol selectivity at 513 K and 70 bar [21], highlighting the better behavior of these metals as nanoparticles instead of as cations.

A theoretical study about the equilibria conditions was carried out to guarantee that equilibria is not conditioning the values obtained. According to Moteki and Flaherty [9], the main mechanism is divided into 14 individual steps (considering both, adsorption and reaction processes), being most of them equilibria steps. According to this proposal, the acetaldehyde productivity could be theoretically conditioned by the ethanol adsorption, the proton abstractions to obtain the ethoxyde and acetaldehyde on the catalytic surface, and their corresponding adsorption-desorption equilibria. Despite the complexity of the analysis of these individual steps, a first approach supposes the acetaldehyde formation as an equilibrium step considering the ethanol and hydrogen in the medium. Thus, experimental results were used to estimate the reaction quotients (Q) and these values were compared to the theoretical equilibrium constant K, obtaining, in the worst case, a Q/K ratio lower than 0.002, suggesting that the reaction is far from equilibrium at these conditions.

Despite the metal used, the general profiles are similar, with a decreasing trend of acetaldehyde, typical evolution of a primary product; and a formation pattern characterized by a maximum and a subsequent decrease for the 1-butanol, that responds to a product obtained after serial steps of a global reaction that continues and produces undesired compounds (if temperature conditions are too severe). One of the main side-products is the ethylene, with a continuous increasing trend, more marked in the case of the bulk material. Consequently, no evidences of any change in the main reaction mechanisms were observed when introducing metals or reducing conditions, allowing the analysis of the influence of metals and reducing conditions.

3.3. Analyses of reactions results

Considering that the aim of this work is to enhance the 1butanol productivity, the good results shown in Fig. 2 can be better illustrated analyzing the influence of metals and reducing conditions on the 1-butanol productivity. Since medium strength basic sites are considered the most active sites for aldol condensation, Fig. 3 shows the 1-butanol productivity under reducing conditions, normalized by the concentration of medium strength basic sites, according to the expression of the α

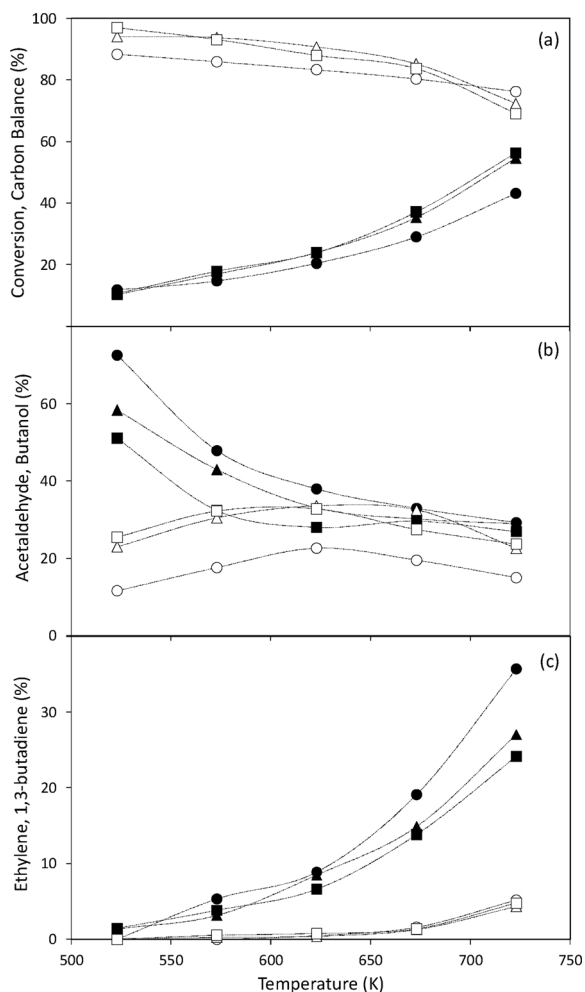


Fig. 2. Catalyst performance at different temperatures under reductive conditions as function of the temperature for the reaction catalyzed by (●) Mg-Al; (▲) Ni/Mg-Al; and (■) Co/MgAl. Results in terms of: (a) conversion (black) and carbon balance (white); (b) acetaldehyde (black) and butanol (white) selectivity; (c) ethylene (black) and 1,3-butadiene (white) selectivity.

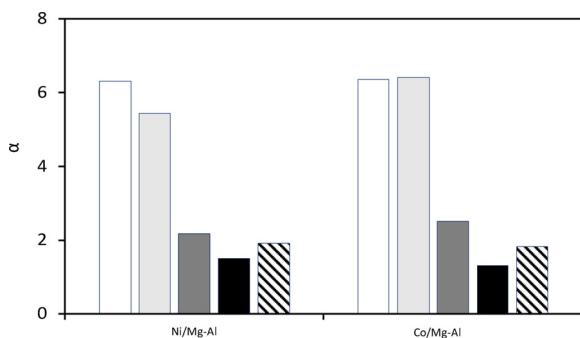


Fig. 3. Comparison of the relative 1-butanol concentration obtained under reducing conditions. Results normalized by the MgAl ones. Values correspond to 523 K (white); 573 K (light grey); 623 K (dark grey); 673 K (black) and 723 K (bars).

parameter, defined as follows:

$$\alpha = \frac{\left(\frac{[\text{butanol productivity}]}{[\text{surface basicity}]_{\text{medium strength}}}_{\text{metal/Mg-Al}} \right)}{\left(\frac{[\text{butanol productivity}]}{[\text{surface basicity}]_{\text{medium strength}}}_{\text{Mg-Al}} \right)} \quad (3)$$

A clear improvement is observed; mainly at the mildest conditions,

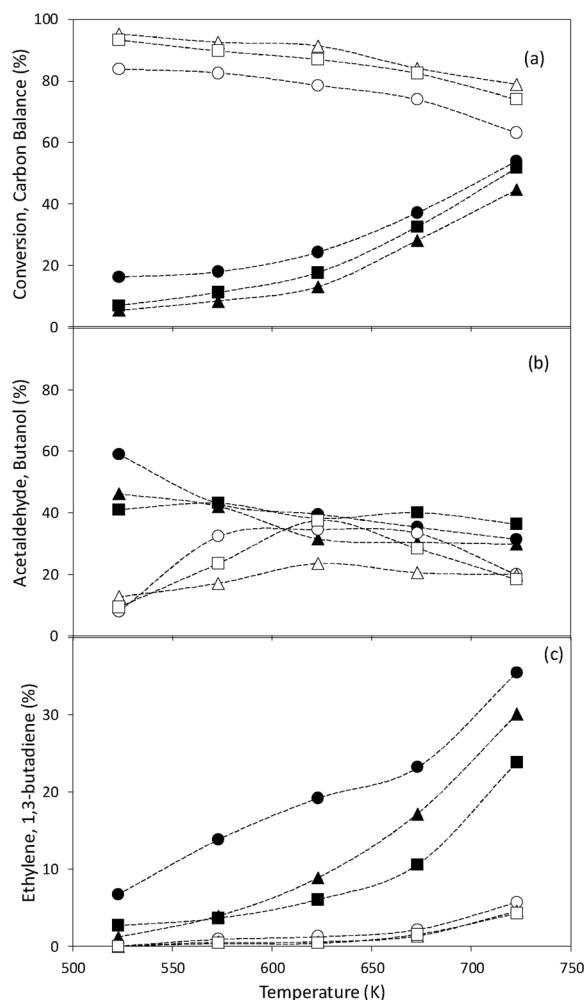


Fig. 4. Catalyst performance at different temperatures under inert conditions as function of the temperature for the reaction catalyzed by (●) Mg-Al; (▲) Ni/Mg-Al; and (■) Co/Mg-Al. Results in terms of: (a) conversion (black) and carbon balance (white); (b) acetaldehyde (black) and butanol (white) selectivity; (c) ethylene (black) and 1,3-butadiene (white) selectivity. Results of Mg-Al correspond to our previous work [20].

which is an extra advantage of this strategy. At the lowest temperature, the α parameter is almost 6 times higher with both metal modified materials than the corresponding one with the Mg-Al, being almost constant with the Co when temperature increases to 573 K. As the temperature increases, the goodness of this configuration decreases, but the productivity is still higher at the highest temperature. These results suggest that the differences between parent and metal-promoted oxides cannot be explained only in terms of their reactivity for aldol condensation (despite this reaction is often considered as the rate-determining step [9,15]). Thus, the role of the catalyst properties on dehydrogenations and hydrogenations must be considered in detail.

In order to get a better understanding on these reactions, strongly dependent on hydrogen concentration, the same set of experiments was performed in absence of hydrogen, being the results depicted in Fig. 4. First step affected by the metal presence is the ethanol dehydrogenation. The global effect of reducing conditions and metal catalyst in this reaction is compared in Fig. 5. For this analysis, AA corresponds to acetaldehyde whereas the term “C4 main route” involves the sum of the yields to crotonaldehyde, crotyl alcohol, butanal, 1-butanol, 1,3-butadiene and ethyl acetate, in order to have an idea of the overall catalytic performance for the ethanol dehydrogenation. A clear increasing trend is obtained in all cases, but significant differences, as function of the materials, are observed when comparing the effect of inert or reducing

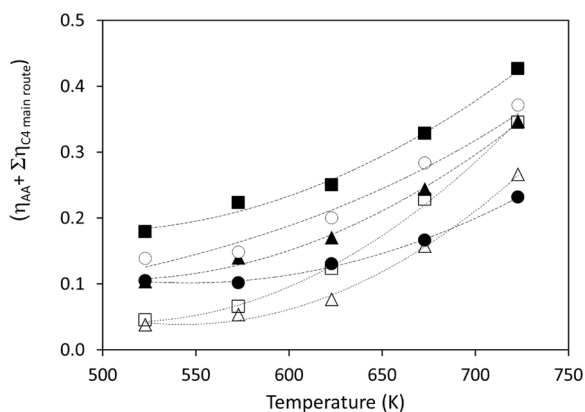


Fig. 5. Analysis of the dehydrogenation capacity as function of the catalyst and reaction temperature. Results under inert (open symbols) and reducing atmosphere (solid symbols). Symbol: Mg-Al (●); Co/Mg-Al (■); Ni/Mg-Al (▲).

atmosphere. When working under inert conditions, best results are obtained using the parent Mg-Al (almost 3 times higher comparing to the bifunctional ones). It should be highlighted the unexpected effect of reducing conditions when Mg-Al is used as catalyst, the presence of hydrogen hindering the reaction. Considering that there is not any metal phase to activate the hydrogen molecule, a similar behavior would be expected. However, there are clear differences that must be directly related to adsorption processes, suggesting a non-dissociative adsorption of hydrogen molecules on the catalytic surface, hindering the ethanol adsorption needed for the aldolization step. This hypothesis is supported by previous works that noticing the H_2 adsorption on acidic sites (OH groups) using similar oxides [35,36]. Trends achieved with the bifunctional materials show higher slope than those observed for the parent Mg-Al. This fact happens since dehydration side reactions are more favored at increasing temperatures, being more relevant when using the bulk MgAl because of its higher acidity (supported by Table 1, and Figs. 2c and 4c) [35].

Concerning the comparison between bifunctional materials, the nickel catalyst reaches the lowest values and its trend shows lower slope than that observed with the cobalt one. This is in agreement with the low concentration and strength of basic sites owned by the Ni/MgAl, together with the preference of this metal for favoring hydrogenations [37]. In presence of hydrogen, the Co/Mg-Al catalyst shows the best dehydrogenation performance, reaching improvements up to of 22 and 87% in regard to the Ni/Mg-Al and Mg-Al materials. Thus, it is confirmed that hydrogen supplying enhances the performance to the main route preceded by ethanol dehydrogenation. This net improvement under reducing atmosphere is explained by the effect of the subsequent steps. It can be supposed that cobalt enhances the consumption of acetaldehyde to produce the C4 compounds, displacing the equilibrium to the formation of more acetaldehyde. In order to check this hypothesis, the following steps must be analyzed.

Fig. 6 illustrates the relative weight of condensation steps, analyzing the aldol condensation (Fig. 6a) and the acetaldehyde transformation into ethyl acetate via Tishchenko-type reaction (Fig. 6b). The highest condensation activity was obtained with Ni/Mg-Al under reducing conditions, with similar values as those obtained with Mg-Al under inert atmosphere. Ni/Mg-Al shows higher aldolization capacity than the expected one, considering the low concentration of basic sites of this material. This analysis suggests that the main role of nickel is to improve the subsequent steps that consume the condensation adduct, shifting the equilibrium. This fact is congruent with the larger improvement observed in presence of hydrogen, relating the profile with the following hydrogenation steps. The different behavior of the cobalt material must be highlighted. With this material, a strong influence of atmosphere is observed, enhancing the ethyl acetate in presence of hydrogen. Both compounds, ethyl acetate and crotonaldehyde, are

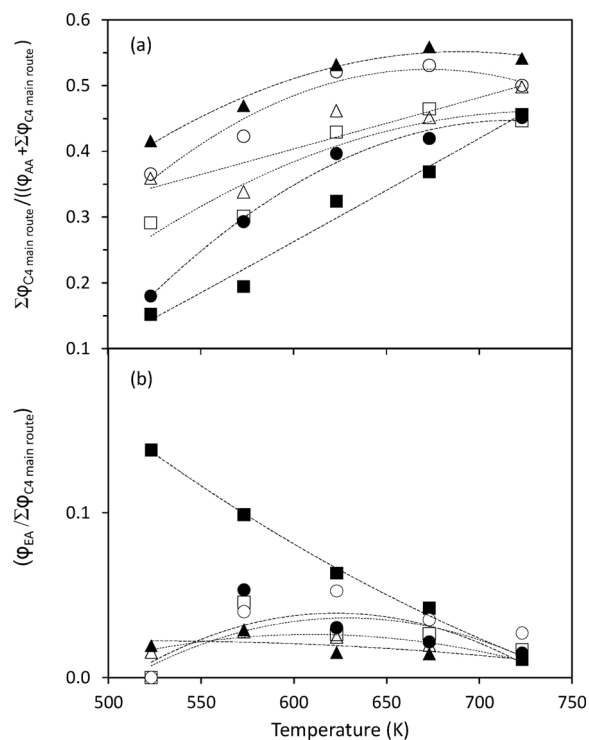


Fig. 6. Analysis of (a) aldol condensation step and (b) acetaldehyde esterification side-reaction, under inert (white) and reducing (black) conditions. See Fig. 5 for symbols.

obtained from ethanol, but involving different intermediates: acyl for the ethyl acetate ($CH_3-C^*=O^*$) and enolate ($CH_2^*-CH=O$) [38]. Results obtained suggest that the presence of hydrogen and cobalt inhibits to some degree the formation of the enolate intermediate from acetaldehyde ($^{\beta}C-H$ scission hindered by hydrogen adatoms), enhancing the selectivity to the esterification pathway, mainly at low temperatures. This is the reason explains the poor aldolization results despite the higher acetaldehyde formation rate with Co-containing material, the most active for dehydrogenation activity.

The study of hydrogenation step is shown in Fig. 7, analyzing the ratio between the 1-butanol selectivity and the selectivity for all the C4 condensation adducts. The different role of each metal is clearly observed in this plot. Ni/Mg-Al catalyst shows the highest adducts hydrogenation activity, mainly under reductive atmosphere, being this positive effect less evident as the temperature increases. On the other hand, the absence of any metal phase limits the hydrogenation activity

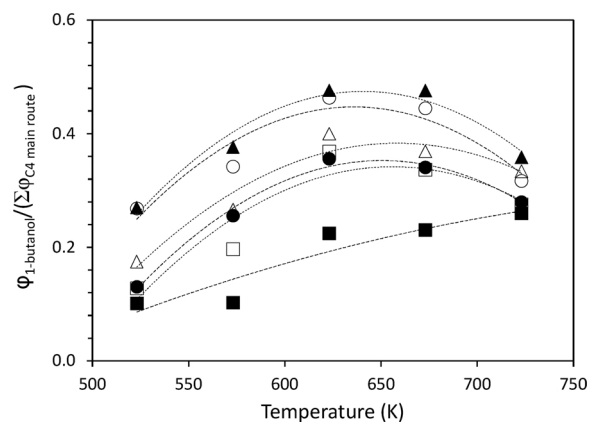


Fig. 7. Analysis of selective hydrogenation to 1-butanol under inert (white) and reducing (black) conditions. See Fig. 5 for symbols.

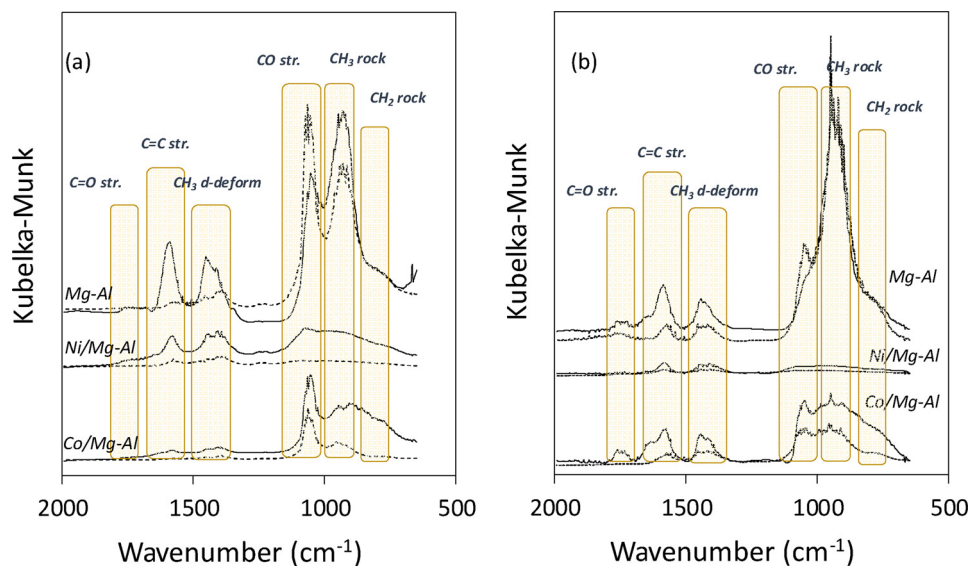


Fig. 8. DRIFT spectra of different catalyst during the ethanol condensation under inert (lines) or reducing conditions (broken lines). Results corresponding to reaction at (a) 573 K and (b) 723 K. Relative intensities of (b) spectra are ten times higher than those observed in the (a) spectra.

of Mg-Al and, as a consequence, hydrogen has not any positive effect when this material is used. Concerning to the Co catalysts, they do not show any noticeable hydrogenation activity, being the obtained results similar or even worse than the corresponding to the parent mixed oxide. The decreasing trend observed in almost all the cases at the highest temperatures is caused by the higher relevance of oligomerization reactions (in good agreement with the observed decrease in the carbon mass balance) and also dehydration to produce 1,3-butadiene at the most severe conditions.

In order to verify all these hypothesis, DRIFT spectroscopy experiments were carried out, trying to identify relevant differences in the adsorption modes of the compounds involved in the reaction as function of the material and atmosphere conditions. DRIFT analyses were carried out at similar conditions as in the reaction medium, being possible the direct comparison of both results. As examples of the most significant results, spectra obtained at 573 K and 723 K are compared in Fig. 8, under inert and reducing conditions.

The same three regions, related to specific functional groups, were observed for all the materials, corroborating that same type of interactions are taken place. The first one is identified as the stretching mode of CO (1050 cm^{-1}) [20], being related to the adsorption of alkoxide species. The second one, at 1580 cm^{-1} corresponds to the stretching vibration mode of C=C bonds (unsaturated alcohols and aldehydes), such as the crotonaldehyde and crotyl alcohol [20]. Under inert atmosphere, highest intensities of these adsorption modes are in good agreement with the highest concentration of acid sites (almost six times higher with Mg-Al than with the bifunctional ones, Table 1), mainly at 723 K. Consequently, aldehydes and alcohols present in the reaction media, mainly the heaviest ones, are adsorbed time enough to promote subsequent reactions yielding heavier compounds [39]. The high decrease of these signals when working under reducing conditions suggest that hydrogen hinders the adsorption of these compounds, avoiding their further reactions. The third band, at 1740 cm^{-1} , is related to the stretching vibration mode of C=O of aldehydes [20]. This band is only observed with MgAl at 723 K under inert conditions, suggesting the presence of relevant amount of crotonaldehyde adsorbed on the catalytic surface. There are other two bands clearly observed, at 950 and 1440 cm^{-1} , approximately. These bands correspond to common vibration modes of CH₃ (rocking and deforming one, respectively) [20], so they are not useful to identify any relevant molecule.

If results under inert and reducing conditions are compared, there is a clear difference between Mg-Al and the metal-modified materials,

mainly Ni. Spectra obtained with the parent material are almost the same, in good agreement with the negligible role of hydrogen in absence of any metal phase. On the contrary, signals generally decrease for the metal-modified catalysts, suggesting that adsorption is less relevant because of the presence of hydrogen and the lower concentration of strong basic and acid sites. Most relevant results are obtained with Ni/Mg-Al under reducing conditions, with almost null interactions related to heavy compounds. This fact corroborates the direct link between hydrogenation activity and hindering permanent adsorption and the consequent oligomerization.

3.4. Overall effect on the 1-butanol productivity

In order to determine the optimal combination of catalyst and reaction conditions to maximize 1-butanol production, Fig. 9 summarizes the 1-butanol productivity. Data shown correspond to an analysis of the different productivity rates, normalizing all the values by the corresponding ones for the bulk material (β), at inert or reducing conditions, defined as:

$$\beta = \frac{[P_{1-butanol}]_{\text{metal/Mg-Al}}}{[P_{1-butanol}]_{\text{Mg-Al}}} \quad (4)$$

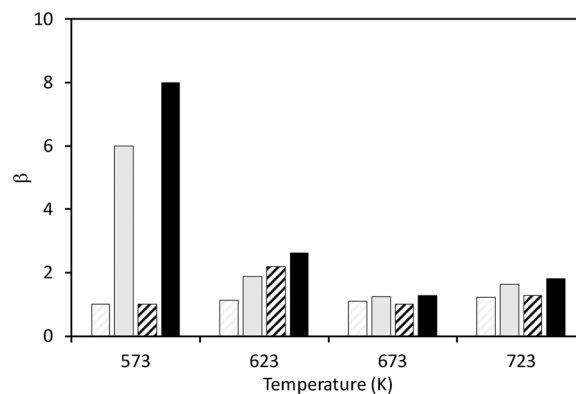


Fig. 9. Comparison of the relative 1-butanol production rate obtained with the different materials under inert (bars) and reducing atmosphere (solid colors). Data normalized as function of results with the bulk MgAl. Values corresponding to Ni (grey) and Co (black) materials.

In global terms, the influence of metals is more relevant at low temperatures, being their effect almost negligible over 673 K. This is also an advantage of this procedure, increasing the green character of this process, obtaining good results at milder conditions than the normally used in the literature [8,11]. At low temperatures, the reducing atmosphere also plays a key role, obtaining relative rates more than six times higher than the obtained under inert atmosphere (in both cases). The highest 1-butanol productivity is reached at 573 K with the Co, with eight rates eight times higher than the one obtained with Mg-Al. Thus, the need of reducing conditions is also justified, observing clear improvements at temperatures too low to produce the hydrogenations by MPV and surface mediated hydrogen-atom transfer mechanisms.

4. Conclusions

According to the deep analysis of the ethanol gasphase condensation, the highest complexity of this mechanism is remarked. As consequence, it is very difficult to determine an optimum material with good properties for all the individual steps. Cobalt highlights by its high dehydrogenation capacity but it also enhances the ethyl acetate production (undesired side reaction). On the other hand, Nickel presents a relevant activity in aldol condensation and a high activity of the C=O and C=C hydrogenation, obtaining the best results for these two stages. In this case, a positive role of hydrogen is clearly observed. Nickel also limits the oligomerization (undesired reaction), as it was observed by DRIFT spectroscopy. Bands related to the adsorption of higher alkoxides are much more relevant with this material, mainly under inert atmosphere.

Thus, the 1-butanol productivity (target compound) is conditioned by the balance of all these stages. Under the conditions tested in this work, the dehydrogenation step controls the final result, obtaining the highest amount of 1-butanol when Co/Mg-Al is used, mainly at low temperature. At these mild conditions, when this reaction prevails over the dehydration and despite the higher amount of ethyl acetate obtained with this material. This improvement is much more relevant under reducing conditions, highlighting also the role of hydrogenation steps. On the other hand, results obtained with Ni/Mg-Al are also relevant, obtaining good productivity of 1-butanol and increasing the global selectivity to the main process (less amount of ethylene, ethyl acetate and oligomers).

Acknowledgments

The authors acknowledge financial support from the Ministry of Economy and Competitiveness of the Government of Spain (Contract: CTQ2014-52956-C3-1-R). Jorge Quesada also thanks for his Ph.D. fellowship (PA-14-PF-BP14-105) of the Severo Ochoa Program of the local Government of the Principality of Asturias.

Appendix A. Supplementary data

Supplementary material related to this article can be found, in the

References

- [1] L. Faba, E. Díaz, S. Ordóñez, *Renew. Sustain Energy Rev.* 51 (2015) 273–287.
- [2] W.E. Taifan, G.X. Yan, J. Baltrusaitis, *Catal. Sci. Technol.* 20 (2017) 4648–4668.
- [3] J.H. Earley, R.A. Bourne, M.J. Watson, M. Poliakoff, *Chem.* 17 (2015) 3018–3025.
- [4] S. Hanspal, Z.D. Young, H. Shou, R.J. Davis, *ACS Catal.* 5 (2015) 1737–1746.
- [5] L. Silvester, J.F. Lamonier, J. Faye, M. Capron, R.N. Vannier, C. Lamonier, J.L. Dubois, J.L. Couturier, C. Calais, F. Dumeignil, *Catal. Sci. Technol.* 5 (2015) 2994–3006.
- [6] S. Ordóñez, E. Díaz, M. León, L. Faba, *Catal. Today* 167 (2011) 71–76.
- [7] J.T. Koslowski, R.J. Davis, *J. Energy Chem.* 22 (2013) 58–64.
- [8] S. Ogo, A. Onda, K. Iwasa, A. Fukuoka, J. Yanigisawa, *J. Catal.* 296 (2012) 24–30.
- [9] T. Moteki, D.W. Flaherty, *ACS Catal.* 6 (2016) 4170–4183.
- [10] A.S. Ndou, N. Plint, N.J. Coville, *Appl. Catal. A* 251 (2003) 337–345.
- [11] T. Tshuchida, J. Kubo, T. Yoshioka, S. Sakuma, T. Takeguchi, W. Ueda, *J. Catal.* 259 (2008) 183–189.
- [12] C.R. Ho, S. Shylesh, A.T. Bell, *ACS Catal.* 6 (2016) 939–948.
- [13] J.I. Di Cosimo, V.K. Díez, M. Xu, E. Iglesia, C.R. Apesteguía, *J. Catal.* 178 (1998) 499–510.
- [14] K.A. Goulas, G. Gunbas, P.J. Dietrich, S. Sreekumar, A. Grippo, J.P. Chen, A.A. Gokhale, F.D. Toste, *ChemCatChem* 9 (2017) 1–10.
- [15] J.T. Koslowski, R.J. Davis, *ACS Catal.* 3 (2013) 1588–1600.
- [16] J. Zaffran, C. Michel, F. Delbecq, P. Sautet, *J. Phys. Chem. C* 119 (2015) 12988–12998.
- [17] M.A. Ortuño, V. Bernales, L. Gagliardi, C.J. Cramer, *J. Phys. Chem. C* 120 (2016) 24697–24705.
- [18] J.J. Ramos, V.K. Díez, C.A. Ferretti, P.A. Torresi, C.R. Apesteguía, J.I. Di Cosimo, *Catal. Today* 172 (2011) 41–47.
- [19] J.I. Di Cosimo, A. Acosta, C.R. Apesteguía, *J. Mol. Catal. A* 222 (2004) 87–96.
- [20] J. Quesada, L. Faba, E. Díaz, S. Ordóñez, *Appl. Catal. A* 542 (2017) 271–281.
- [21] T. Riitonen, K. Eränen, P. Mäki-Arvela, A. Shchukarev, A.R. Rautio, K. Kordas, N. Kumar, T. Salmi, J.P. Mikkola, *Renew. Energy* 74 (2015) 369–378.
- [22] J.J. Bravo-Suárez, B. Subramaniam, R.V. Chaudhari, *Appl. Catal. A* 455 (2013) 234–246.
- [23] J. Pang, M. Zheng, L. He, L. Li, X. Pan, A. Wang, X. Wang, T. Zhang, *J. Catal.* 344 (2016) 184–193.
- [24] X. Wu, G. Fang, Z. Liang, W. Leng, K. Xy, D. Jiang, J. Ni, X. Li, *Catal. Commun.* 100 (2017) 15–18.
- [25] I.C. Marcu, N. Tanchoux, F. Fajula, D. Tichit, *Catal. Lett.* 143 (2013) 23–30.
- [26] M. León, E. Díaz, A. Vega, S. Ordóñez, A. Auroux, *Appl. Catal. B* 102 (2011) 590–599.
- [27] J. Quesada, R. Arreola-Sánchez, L. Faba, E. Díaz, V.M. Rentería-Tapia, S. Ordóñez, *Appl. Catal. A* 551 (2018) 23–33.
- [28] J. Siritá, S. Phanichphant, F.C. Meunier, *Anal. Chem.* 79 (2007) 3912–3918.
- [29] P. Burattin, M. Che, C. Louis, *J. Phys. Chem. B* 102 (1998) 2722–2732.
- [30] I. Obregón, I. Gandarias, A. Ocio, I. García-García, N. Álvarez de Eulate, P.L. Airas, *Appl. Catal. B* 210 (2017) 328–341.
- [31] K.L. Luska, P. Miglowski, S.E. Sayed, W. Leitner, *A.C.S. Sustain. Chem. Eng.* 4 (2016) 6186–6192.
- [32] A. Parmaliana, F. Arena, F. Frusteri, N. Giordano, *J. Chem. Soc. Faraday Trans.* 86 (1990) 2663–2669.
- [33] O.O. James, D. Maity, J. Pet, *Technol. Altern. Fuels* 7 (2016) 1–12.
- [34] E.I. Gürbüz, D. Hibbitts, E. Iglesia, *J. Am. Chem. Soc.* 137 (2015) 11984–11995.
- [35] H.U. Blaser, A. Schnyder, H. Steiner, F. Rössler, P. Baumeister, 2nd ed., G. Ertl, H. Knözinger, F. Schüth, J. Weitkamp (Eds.), *Handbook of Heterogeneous Catalysis*, vol. 7, Wiley VCH, Weinheim, 2008p. 3286.
- [36] J.I. Di Cosimo, C.R. Apesteguía, M.J.L. Ginés, E. Iglesia, *J. Catal.* 190 (2000) 261–275.
- [37] D.D. Eley, M.A. Zammit, *J. Catal.* 21 (1971) 377–383.
- [38] M.E. Sad, N. Neurock, E. Iglesia, *J. Am. Chem. Soc.* 133 (2011) 20384–20398.
- [39] D. Leckel, *Energy Fuel* 21 (2007) 662–667.